Available online at www.sciencedirect.com

SciVerse ScienceDirect

Ceramics International 39 (2013) 5415–5425

CERAMICS INTERNATIONAL

www.elsevier.com/locate/ceramint

Two step hot pressing sintering of dense fine grained WC–Al_2O_3 composites

Haixia Qu[a], Shigen Zhu[a,b,*]

[a]College of Mechanical Engineering, Engineering Research Center of Advanced Textile Machinery, Ministry of Education, Donghua University, Shanghai 201620, PR China

[b]College of Material Science and Engineering, Donghua University, Shanghai 201620, PR China

Received 24 November 2012; received in revised form 12 December 2012; accepted 13 December 2012
Available online 22 December 2012

Abstract

WC–40 vol% Al_2O_3 composites were prepared by high energy ball milling and the following two step hot pressing sintering (TSS). The tungsten carbide (WC) and commercial alumina (Al_2O_3) powders composed of amorphous Al_2O_3, boehmite (AlOOH) and χ-Al_2O_3 were used as the starting materials. The feasibility of two step sintering (TSS) method to WC–40 vol% Al_2O_3 composites was demonstrated, optimum TSS regime was discussed and phase transformation during TSS process was investigated. The results showed that both the pre-sintering at a proper first step temperature (T_1) to obtain a critical initial density and isothermal hot pressing at an appropriate second step temperature (T_2) to inhibit grain boundary migration (GBM) were of significant importance. When the as milled WC–40 vol% Al_2O_3 powders were hot pressed under TSS_4 regime, a relative density of 99% and a grain size of 2.38 μm were obtained, an excellent Vickers hardness of 19.71 GPa was achieved, combining a fracture toughness of 12 MPa $m^{1/2}$ with a flexural strength of 1285 MPa. Compared with the near full dense samples consolidated under CS_1 regime (1540 °C for 90 min), the grain size decreased, the Vickers hardness, fracture toughness and flexural strength were all improved due to the refined microstructure and the transgranular fracture mode. The amorphous Al_2O_3, AlOOH and χ-Al_2O_3 were transformed to α-Al_2O_3 completely during the sintering process.

Keywords: A. Two step hot pressing; B. Microstructure-final; C. Mechanical properties; D. WC–Al_2O_3 composites

1. Introduction

Sintering methods play a major role in developing high density ceramics with fine grain size. Nowadays, conventional sintering (CS), spark plasma sintering (SPS), hot isostatic pressing sintering (HIP) and microwave sintering (MW) have already been employed to obtain nearly full dense ceramics. These sintering methods proceed through diverse mechanisms and densification kinetics, it is possible to acquire sintered ceramics with desired microstructure. However, it is difficult to achieve full densification without promoting grain growth. So it is important to choose a promising consolidation technique to avoid exaggerated grain growth at the final stage of sintering.

In order to consolidate samples with full densification and finer grain size, the conventional sintering regime should be modified which have been investigated earlier by rate controlled sintering (RCS) and recently by two step sintering (TSS) [1–4]. Chen and Wang have proposed a novel two step sintering (TSS) method which exploits the difference in kinetics between the grain boundary diffusion (GBD) and grain boundary migration (GBM) in the final sintering stage to suppress grain growth while promoting densification [4]. This method of sintering consists of two steps in the heating schedule. In the first step of TSS, samples should be heated to a higher temperature (T_1), which has to be high enough to achieve critical density at which pores become thermodynamically unstable against

*Corresponding author at: College of Mechanical Engineering, Engineering Research Center of Advanced Textile Machinery, Ministry of Education, Donghua University, Shanghai 201620, PR China. Tel./fax: +86 21 6779 2813.
E-mail addresses: sgzhu@dhu.edu.cn, qhx4001@163.com (S. Zhu).

0272-8842/$ - see front matter © 2012 Elsevier Ltd and Techna Group S.r.l. All rights reserved.
http://dx.doi.org/10.1016/j.ceramint.2012.12.049

shrinkage. After short holding at T_1, the temperature must be immediately lowered to T_2 at which GBM is suppressed while GBD could be continued [4]. Until now, the TSS method is successfully applied to prepare dense fine grained materials with enhanced mechanical, electrical or magnetic properties, such as Y_2O_3 [4,5], $BaTiO_3$ [6], Ni–Cu–Zn ferrites [6], ZnO [7], TiO_2 [8], $8Y_2O_3$ stabilized ZrO_2 [9], Y-TZP [10], Al_2O_3 [11,12], alumina–zirconia ceramics [13], Yttrium aluminum garnet (YAG) transparent ceramics [14], corundum abrasives [15], oxide ceramics with different crystal structure [16], forsterite [17], $NiFe_2O_4$ nanopowder compacts [18], biphasic calcium phosphate bioceramics [19], TiO_2 [20], Nd–Fe–B [21], WC–MgO [22] as well as SiC [23] and WC–Co liquid phase sintering [24].

WC–Al_2O_3 composites have been successfully consolidated by conventional hot pressing, saving the rare, expensive and strategic resource of Co and developing novel WC matrix materials with high mechanical properties [25]. To improve the mechanical properties of WC–Al_2O_3 composites, additives of MgO and CeO_2 have been added to WC–Al_2O_3 composites, the results show that proper content of additives could refine the microstructure, improve the relative density and bonding strength of WC–Al_2O_3 composites. However, excessive amount of additives could segregate on the grain boundaries and deteriorate the mechanical properties [26]. According to the Orowan-Petch plot [27] and Griffith's theory [28], a small grain size favours a high strength. The decreasing of grain size provides a possibility for enhancing the mechanical properties of WC–Al_2O_3 composites. To the best of our knowledge, until now, there are no published papers dealing with the synthesis of WC–Al_2O_3 composites by two-step hot pressing sintering.

In this paper, the feasibility of densification without grain growth by two-step hot pressing sintering is demonstrated in WC–Al_2O_3 composites. The optimum first step temperature (T_1) and second step temperature (T_2) of the TSS regime are clarified, the influence of different TSS regimes on the evolution of the microstructure and mechanical properties are investigated, and possible mechanism is evaluated.

2. Experimental procedure

2.1. Nanopowder preparation and characterization

Nanocrystalline WC–40 vol% Al_2O_3 was synthesized via mechanical alloying process. Commercial powders of WC (74 μm, 99% purity, Sinopharm Chemical Reagent Co. Ltd.) and Al_2O_3 (composed of AlOOH, χ-Al_2O_3 and amorphous Al_2O_3; 150 μm, Sinopharm Chemical Reagent Co. Ltd.) were mixed and ball milled using a QM-1SP4 planetary ball milling machine under argon gas atmosphere for 50 h. The ball to powder weight ratio was 10:1 and the rotation speed of the mill was 350 revolutions per minute (rpm). Both the vial and milling balls (10 mm in diameter) were made of cemented carbide materials.

The phase identification of the as milled powders were investigated by X-ray diffraction (XRD) using a D/max-2550PC (Rigaku Co., Japan) X-ray diffractometer with a Cu K_α radiation ($\lambda = 0.15418$ nm) at 40 kV and 200 mA. The microstructure of the as milled powders and sintered samples were characterized by S-4800 (Hitachi Co., Japan) field emission scanning electron microscope (FE-SEM) and JEOL JEM-2100 F Transmission Electron Microscope (TEM).

2.2. Conventional hot pressing and two step sintering

The as milled powders were consolidated under the conventional sintering (CS) and two step hot pressing sintering (TSS) using a vacuum hot pressing furnace (ZT-40-20YB, Shanghai Chen Hua Electric Furnace Co. Ltd.) under a pressure of 39.6 MPa (applied already from the start) in a vacuum (about 1.3×10^{-1} Pa) atmosphere. The heating rate of the hot pressing was 10 °C/min. Carbonic paper with a thickness of 0.2 mm was used to prevent adhesion between powders and the die. The thermoelectric couple and infrared thermometer were selected to measure the temperature, located in the surface of the mold. The conventional hot pressing sintering (CS_1), 3 min holding sintering (CS_2) and the two step hot pressing sintering (TSS) were implemented as follows:

(1) *Conventional hot pressing sintering* (CS_1): CS_1 were carried out in the temperature range of 1450–1750 °C for 90 min, respectively, with 50 °C temperature intervals [25]. The grain size and relative densities of these samples were compared with that of the samples obtained via TSS regimes to evaluate the beneficial effect of the TSS regimes.
(2) *3 min holding sintering* (CS_2): This sintering was conducted in the temperature range of 1450–1800 °C with 50 °C temperature intervals. The specimens were held at the highest temperature for 3 min in order to obtain a uniform temperature throughout the samples. The first step temperature (T_1) and the second step temperature (T_2) of the TSS regimes were designed according to the grain size and relative densities of these samples.
(3) *Two step hot pressing sintering* (TSS): TSS was carried out under the same conditions as the CS. Samples were firstly heated to a higher temperature T_1, held at T_1 for 3 min (t_1) and then immediately cooled to a lower temperature T_2 and held at T_2 for various time (t_2). The cooling rate of TSS between T_1 and T_2 was 60 °C/min. The samples were held at T_2 up to 6 h so as to reach a higher density. The sintering schedules designed in this experiment were summarized in Table 1.

2.3. Characterization of the hot pressed samples

For each hot pressing regime, more than one sample were consolidated and characterized under the same condition. The hot pressed samples were ground and polished

by standard ceramographic methods. The phase identification of the sintered samples was investigated by X-ray diffraction (XRD) as the as milled powders. The microstructure of the sintered samples was characterized by S-4800 (Hitachi Co., Japan) field emission scanning electron microscope (FE-SEM) and Nanoscope IV (Veeco Co., USA) scanning probe microscope (SPM). Then the samples were etched in Murakami's reagent consisting of $Fe_3[K(CN)_6]$ (10 g), KOH (10 g) and distilled water (100 ml) for 5 min to expose the grain boundary of WC. The polished and etched samples were characterized by a JSM-5600LV (JEOL Co., Japan) scanning electron microscope (SEM).

The densities of the sintered samples were measured using water immersion method in accordance with Archimedes' principle. The hardness of sintered specimens (the average of 10 indentations) was determined using a HVS-50Z Vickers indenter with a load of 30 kg and a dwell time of 10 s. The crack shapes of the specimen determined by repeated surface polishing were confirmed to be Palmqvist crack pattern and in accordance with the Shetty's model, so the fracture toughness (K_C) calculations were based on the crack length measurement of the radial crack pattern produced by Vickers indentations according to the formula estimated by Shetty et al. [29]. The fracture toughness values were derived from the average of 10 measurements. The flexural strength of sintered samples was measured by the three-point flexural test method at room temperature according to the ASTM B312 standard. The samples were cut, ground and polished into $3 \times 5 \times 15\ mm^3$ specimens. The three-point flexure tests were carried out on a WDW-100 (Changchun kexin experimental equipment Co. Ltd., China) test machine with a span of 10 mm and cross-head speed of 0.01 mm/min. The fracture strength of sintered samples (the average of at least six tests) was calculated using

$$\sigma = 3PL/2t^2w \quad (1)$$

where σ (MPa) is the flexural fracture strength, P (N) is the force required to rupture, L ($L=10$ mm) is the length of the span of fixture, w ($w=5$ mm) is the width of the specimen, and t ($t=3$ mm) is the thickness of the specimen.

3. Results and discussion

3.1. Nanopowder characterization

The morphology of the as milled WC–40 vol% Al_2O_3 powders were shown in Fig. 1. From the bright field images (BFI) it can be seen that the dark grains and gray grains are WC and Al_2O_3 and the particle size varied from 47 to 573 nm in diameter. The diffuse diffraction rings indicate the existence of amorphous Al_2O_3 in the as milled powders and the much stronger diffraction lines stand for the crystalline parts of WC, as shown in Fig. 1b, obviously, it can be indicated the fine crystal structure of WC as well.

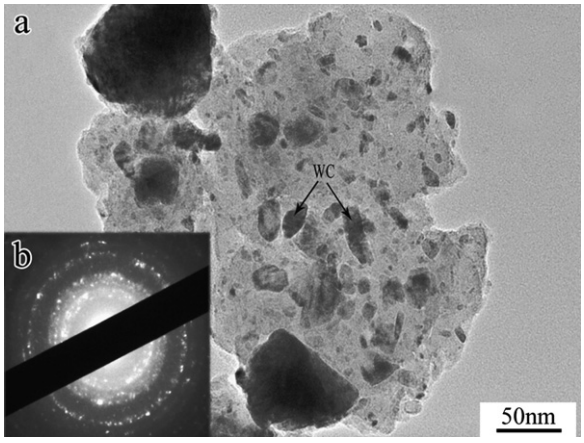

Fig. 1. (a) BFI and (b) the corresponding SADP of the WC–40 vol% Al_2O_3 powders ball-milled for 50 h.

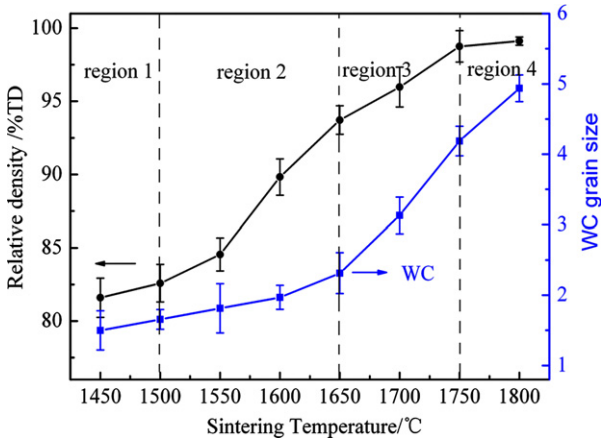

Fig. 2. Relative density and grain size of WC–40 vol% Al_2O_3 composites as a function of sintering temperature under 3 min holding sintering.

According to our previous XRD analysis work [25], the commercial Al_2O_3 starting powders were consisted of a great quantity of amorphous Al_2O_3 and trace amounts of AlOOH and χ-Al_2O_3. During the ball milling for 50 h, no composition changes took place, and phase transformation of AlOOH, χ-Al_2O_3 and amorphous Al_2O_3 did not occur. Only the decreased WC crystalline size was achieved according to the broadened and intensity decreased WC peaks.

3.2. Conventional hot pressing

The relative density and WC grain size versus the sintering temperature under 3 min holding conventional hot pressing sintering were shown in Fig. 2. It could be seen that, the change of the relative density and WC grain size as a function of the sintering temperature showed four distinct regions. In region 1, in other words, when the temperature was below 1500 °C, there was no obvious change in the relative density and grain size. The low densification rate and grain growth rate in region 1 was

attributed to the low temperature and short holding time. The GBM was not allowed and the GBD did not have enough time to occur.

In the temperature range of 1500–1650 °C (region 2), the relative density increased (from 83% to 94%TD) while no significant grain growth occurred. The difference between the densification kinetics and grain growth kinetics of WC–Al_2O_3 composites guaranteed the feasibility of the TSS on the compacts. As a result, region 2 was the optimum temperature range for T_1.

When the temperature increased from 1650 °C to 1750 °C in region 3, the relative density changed from 94%TD to 99%TD while the WC grain size increased from 2.31 μm to 4.19 μm. That is, 5.38% increase of relative density led to remarkable WC grain growth of more than 80%. The fast increase of grain size as well as less evident densification rate was attributed to the final stage and the coarsening of the grains. Collapse of open pore structure in the final sintering stage resulted in the substantial decrease in pore pinning effect and the accelerated grain growth [30].

In the temperature region 4, it was clear that further increase in temperature (from 1750 °C to 1800 °C) resulted in a slight density enhancement, however, with an obvious increase in the grain size. The exhausting densification rate in region 4 was associated with the coarsening of grains in the final sintering stage.

As a result, according to the quick densification rate and slow grain growth rate, 1600 °C and 1650 °C with the relative density of 90%TD and 94%TD, respectively, were selected as the first step temperature (T_1) of the TSS regimes. The second step temperature (T_2) was set in the range of 1400–1500 °C. The TSS regimes were shown in Table 1.

3.3. Two step sintering

The as milled WC–40 vol% Al_2O_3 powders were firstly consolidated under TSS_1 and TSS_{41} (1600 °C/3 min→1450 °C/2 h) regimes to determined the optimum first step temperature (T_1) according to their properties. The relative density (ρ_1) and grain size (d_1) of the TSS_1 samples and that of TSS_{41} samples were shown in Fig. 3c. From Fig. 3c, it could be indicated that although the relative density of the TSS_1 samples was higher than that of TSS_{41} samples due to the higher first step sintering temperature, the grain size of the TSS_1 samples was larger than that of TSS_{41} sample, as a result, the mechanical properties of the TSS_1 sample was lower than that of TSS_{41} sample, indicating that 1650 °C was too high to be chose as the first step temperature, and 1600 °C with large densification rate and small grain growth rate was the proper first step temperature.

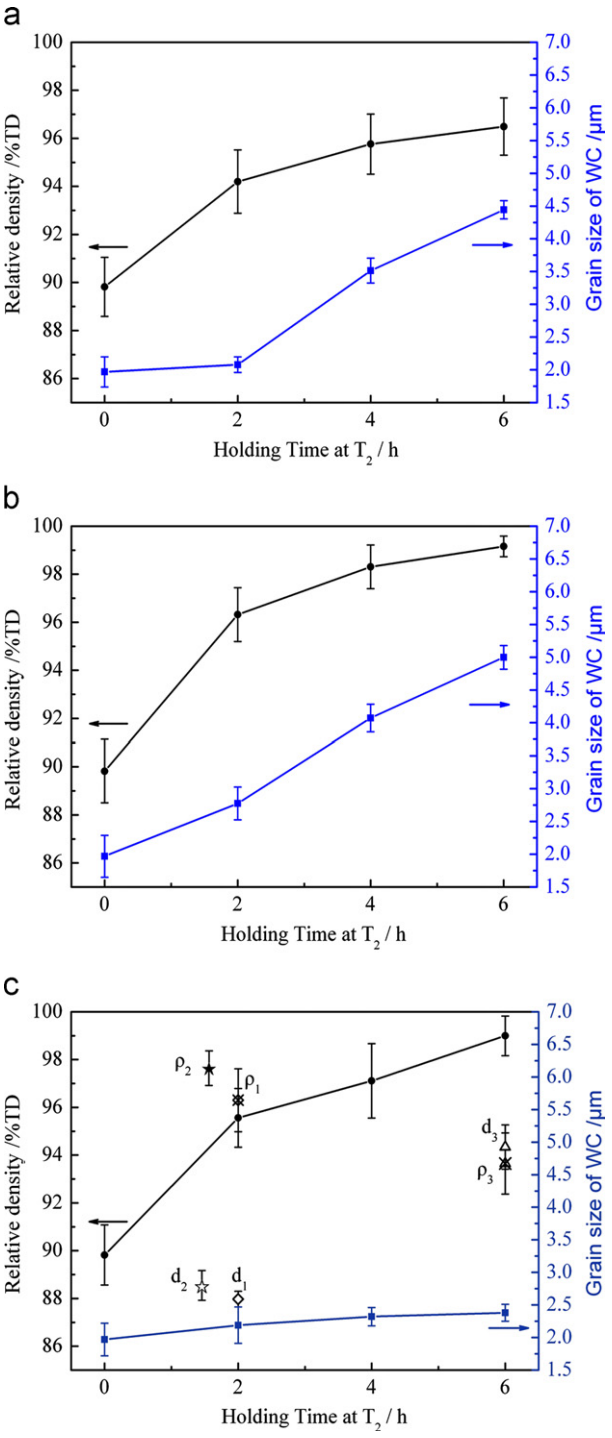

Fig. 3. Relative density and grain size versus holding time at (a) 1400 °C (TSS_2), (b) 1500 °C(TSS_3) and (c) 1450 °C(TSS_4) for WC–40 vol% Al_2O_3 composites firstly heated up to 1600 °C.

Table 1
Two step hot pressing sintering schedules designed in this experiment.

Regimes	T_1 (°C)	T_2 (°C)	Holding time at T_2 (h)
TSS_1	1650	1450	2
TSS_2	1600	1400	2–4–6
TSS_3	1600	1500	2–4–6
TSS_4	1600	1450	2–4–6

According to Chen and Wang [4], when the relative density reached 75%TD for Y_2O_3, pores became subcritical

and unstable against shrinkage. The dispersed open pores could pin grain boundaries and hinder grain boundary migration, for which the grain growth was suppressed. However, a relative density higher than 85%TD was necessary for SiC ceramics [23], and in the case of alumina, a relative density of 92% TD was needed to obtain closed porosity [31]. Our experiment had shown that 75%TD was not sufficient in the case of the WC–40 vol% Al_2O_3 composites, and a relative density of at least 90%TD must be achieved before the second low temperature sintering step was applied.

Fig. 3a shows the relative density and grain size versus holding time at 1400 °C for WC–40 vol% Al_2O_3 composites firstly heated up to 1600 °C (TSS_2). When the holding time at 1400 °C increased from 0 to 2 h, rapid densification and no remarkable change of the grain growth were observed. However, holding the specimen for a period from 2 to 6 h at 1400 °C indicated obvious grain growth from 2.08 μm to 4.44 μm while no remarkable change in the final relative density which only reached 96%TD at last. The reason for the stops of the densification before achieving fully density in TSS_2 was attributed to the low T_2, at which the surface diffusion (SD) was the main sintering mechanism [4]. To confirm the main sintering mechanism of 1400 °C, samples were conventionally hot pressed at 1400 °C. The relative density was 85%TD with little improvement even the holding time was increased to 6 h, and a finger-like growth of WC particles occurred, indicating that the sintering mechanism via SD was performed at 1400 °C through the diffusions of atoms along the surface of nearby particles [13]. At the T_2 lower than the critical one, SD contributed to grain growth without densification. Densification mechanisms such as GBD and volume diffusion (VD) were not active. Densification occurring only when the distances between the centers of the crystallites were diminished, of course, would be impossible without GBD and VD [7]. As a result, when the samples were consolidated under TSS_2 regime, the noticeable grain growth coincided with the densification exhaustion were obtained.

The relative density and grain size evolution of the samples firstly heated up to 1600 °C then followed by sintering at 1500 °C for up to 6 h (TSS_3) were illustrated in Fig. 3b, both the relative density and grain size increased dramatically. With the increasing holding time, a nearly full density of 99%TD was achieved while a significant grain growth from 2.78 μm to 5 μm was observed, that is, coarse structure with a much larger grain size than that of the samples achieved under CS_1 (1540 °C for 90 min, 2.79 μm) was obtained. As shown in Figs. 3c, ρ_2 and d_2 indicated the relative density and the grain size of the samples sintered at 1540 °C for 90 min. The grain size increased continuously with densification during the sintering of the TSS_3 regime attributed to the active GBM at the higher T_2 of 1500 °C.

Fig. 3a and b illustrated how important the T_2 might be. Low T_2 of 1400 °C failed to eliminate the residual porosity, but high T_2 of 1500 °C led to an uncontrolled grain growth. Accordingly, there was a critical temperature of 1450 °C proper for T_2.

Under the TSS_4 regime, T_1 and T_2 were 1600 °C and 1450 °C. The relative density and the grain size as a function of the holding time at T_2 was shown in Fig. 3c. As indicated in Fig. 3c, a nearly full density of 99% was obtained; holding the samples at T_2 led to a remarkable densification (from 96%TD to 99%TD) while no obvious grain growth (from 2.19 μm to 2.38 μm). Compared with the relative density (98%TD) and grain size (2.79 μm) of the samples consolidated under CS_1, samples under the TSS_4 regime had a higher relative density (99%) while a decreased grain size (2.38 μm), as a result, improved mechanical properties were obtained, as shown in Table 2. This result demonstrated the feasibility and highlighted the successful role of two step sintering method on the WC-40 vol% Al_2O_3 composites.

The successful effect of TSS_4 regime could be attributed to the selection of proper T_1 at which a critical density could be reached and the optimum T_2 at which grain growth was inhibited while the densification could be continued. Accelerated grain growth in the final stage of CS was due to the collapse of open pores which could suppress grain growth by pinning grain boundaries and hindering GBM to form closed pores, resulting in the substantial decrease in pore pinning effect, trigging the accelerated grain growth [9]. While under TSS_4 regime, after the first step sintering, pores become subcritical and unstable against shrinkage during the second step sintering, the fine and uniform pore microstructure, which minimized diffusion distance, could maximize densification kinetics and bring the microstructure to the full dense state. On the other hand, GBM dominated by grain boundary mobility at higher temperature was controlled by the junction mobility at lower temperature. During the

Table 2
Mechanical properties of WC–40 vol% Al_2O_3 composites sintered under CS and TSS regimes.

Sintering method	Regimes	Sintering conditions (temperature/holding time)	Vickers hardness HV_{30} (GPa)	Fracture toughness K_C (MPa $m^{1/2}$)	Flexural strength σ (MPa)
CS	CS_1	1540 °C/90 min [4]	18.65 ± 0.57	10.43 ± 0.68	756 ± 33
	CS_3	1450 °C/6 h	16.43 ± 0.26	9.82 ± 0.41	748 ± 57
TSS	TSS_2	1600 °C/3 min → 1400 °C/6 h	18.89 ± 0.31	11.17 ± 0.60	1125 ± 20
	TSS_3	1600 °C/3 min → 1500 °C/6 h	19.60 ± 0.24	11.37 ± 0.65	1149 ± 36
	TSS_4	1600 °C/3 min → 1450 °C/6 h	19.71 ± 0.27	12.00 ± 0.37	1285 ± 47

second step sintering of the TSS_4 regime, the junction became immobile and junction drag occurred, so the GBM was suppressed inhibiting the grain growth successfully [9], accompanying the GBD, the samples combining a nearly full density and a small grain size were obtained.

Fig. 4 shows the grain size-density trajectories, summarizing the effects of different sintering regime of WC–40 vol% Al_2O_3 composites on the densification and grain growth processes. Results of CS_1 were also added [25]. It can be seen that with a holding time of 90 min, the density reached 96% TD even when the sintering temperature was only 1440 °C. With the increasing of sintering temperature, a typical parabolic grain size-density trajectory curve was observed, indicating that the grain size increased continuously with the densification. The nearly full density of 99% TD was achieved in the sample sintered at 1750 °C for 90 min, however, with an obvious large grain size of 6.42 μm, consisting with the common sintering experience that the final stage of densification was normally accompanied by fairly appreciable grain growth [32].

The grain size-density trajectory curve of CS_2 was much more flatted compared with that of the CS_1, as could be seen in Fig. 4. Due to the short holding time of CS_2 regime, the grain growth was inhibited by the high porosity. The grain size of CS_2 sample at nearly full density was finer than that of the CS_1 sample, because for the powder systems in which the activation energy for densification was greater than that for grain growth, fast heating to high temperature could lead to high dense and fine grain sized microstructure.

When the TSS_4 regime was applied to the samples, the significant grain growth usually occurring during the final stage of densification was absent. With the increasing holding time from 2 h to 6 h at T_2 of 1450 °C, the relative density reached 99%, while the grain size was only 2.38 μm. From the grain size/density trajectory of TSS_4 regime, it was indicated that TSS_4 regime resulted in nearly full dense specimens with the smallest average grain size compared to CS_1 and CS_2 regimes. This means that TSS_4 was capable of producing a nearly full dense microstructure accompanied by a suppressed grain growth. Accordingly, improved mechanical properties were obtained.

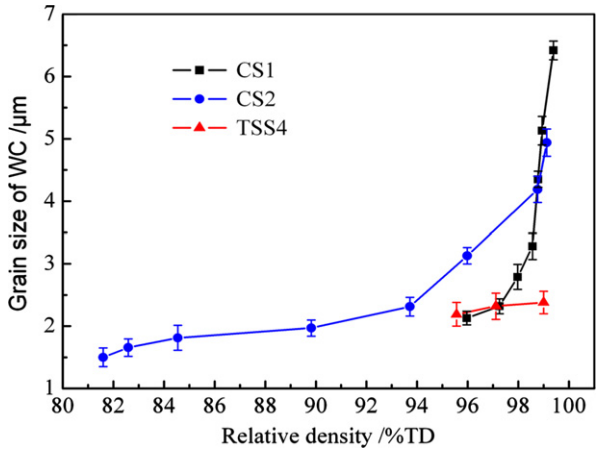

Fig. 4. Grain size-density trajectories of the WC–40 vol% Al_2O_3 composites sintered through various regimes.

3.4. Microstructure evolution in two step sintering process

The backscatter electronic (BSE) FE-SEM images of the polished WC–40 vol% Al_2O_3 composites consolidated under CS_1 regime (1540 °C for 90 min), TSS_4 regime (T_1=1600 °C for 3 min, T_2=1450 °C for 6 h) and CS_3 regime (1450 °C for 6 h) were shown in Fig. 5, showing the different matrix and particulates morphologies of the samples after sintering under different regimes. According to the EDS analysis, the black region contrasts Al_2O_3 and the white region contrasts matrix WC. The backscatter electronic (BSE) FE-SEM images of the fracture surface of WC–40 vol% Al_2O_3 composites consolidated under different sintering regimes were shown in Fig. 6.

Compared Figs. 5a and 6a with Figs. 5b and 6b, respectively, it can be seen that the refined microstructure and reduced grain size were obtained in the samples under TSS_4 regime. According to Fig. 3c, the obviously increased relative density of the samples under TSS_4 regime was higher than that of the samples consolidated under CS_1 regime. This could be explained with the model created by Zhao and Harmer [33–35]. For the final sintering of the ceramics materials, the rate ratio (r) can be defined as the quotient of densification rate and grain growth rate. If $r > 1$, the densification rate would exceed the grain growth rate and the piece would densify. If $r < 1$, the grain growth rate would exceed the densification rate and abnormal grain growth could occur, inhibiting densification. During the early CS process, rapid densification occurred with slight grain growth. However, when density reached 80%–90% TD, the grain size began to increase quickly and densification slowed, which resulted in the decrease of r. Therefore, the discontinuous growth of grains can be detected, and the density was not very high. While, during the TSS process, the relative density reached critical values first which could favor the densification process. Then the TSS_4 regime could enable the value of r to a greater possible extent, and make sure the further densification to a higher value without fast grain growth. Hence, samples consolidated under TSS_4 regime were found to be uniform and compact with smaller grain size.

To emphasis the importance of T_1, the as milled powders were hot pressed at 1450 °C for 6 h under the CS method (CS_3). The polished microstructure and fracture surfaces of CS_3 samples were shown in Figs. 5c and 6c. As shown in Fig. 5c, some pores could be observed on the polished surface of the samples, indicating that the relative density of the CS_3 sample (ρ_3 in Fig. 3c) was lower than that of the TSS_4 samples, while as could be seen in Fig. 6c, the grain size (d_3 in Fig. 3c) was larger than that of the TSS_4 samples. It could be illustrated that the samples without the pre-sintering at the first step sintering (T_1) could not achieve a full density and inhibit the grain growth.

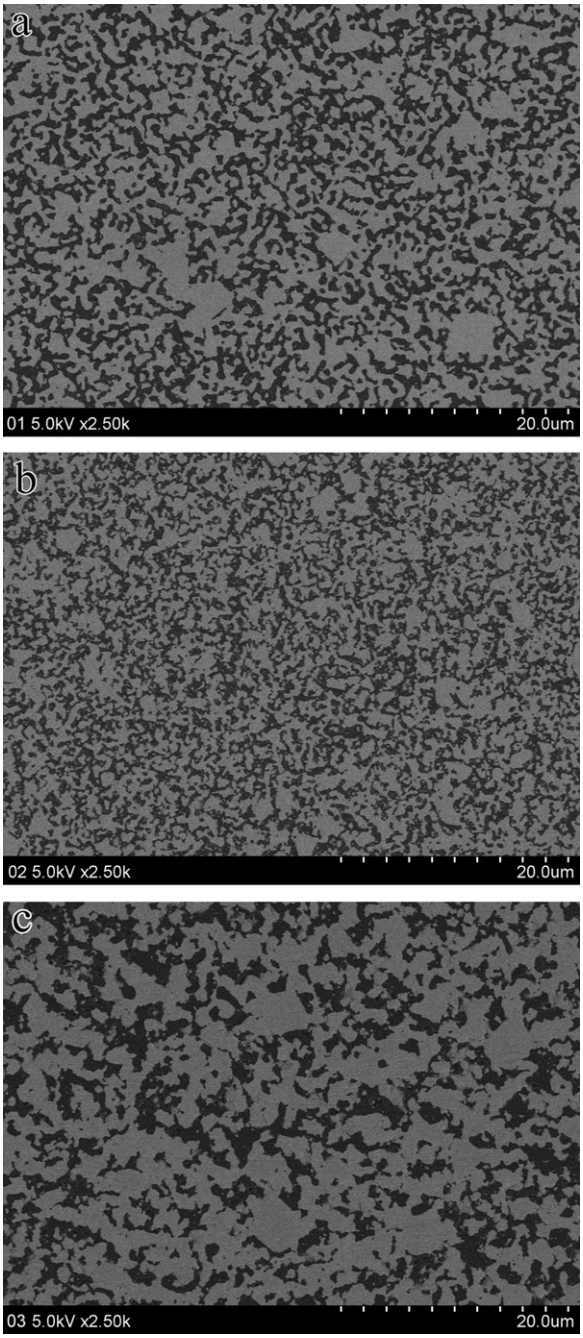

Fig. 5. Backscatter electronic (BSE) FE-SEM images of the polished WC–40 vol% Al_2O_3 composites consolidated under (a) CS_1 regime (1540 °C for 90 min), (b) TSS_4 regime (T_1=1600 °C for 3 min, T_2=1450 °C for 6 h) and (c) CS_3 regime (1450 °C for 6 h).

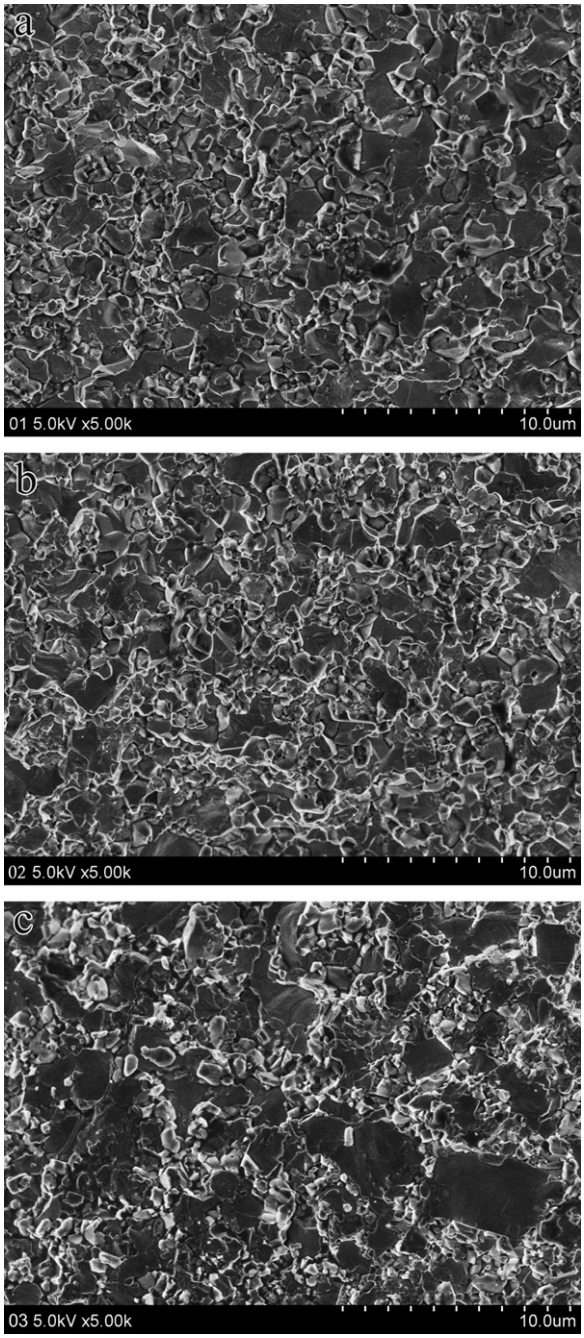

Fig. 6. Backscatter electronic (BSE) FE-SEM images of the fracture surfaces of WC–40 vol% Al_2O_3 composites consolidated under (a) CS_1 regime (1540 °C for 90 min), (b) TSS_4 regime (T_1=1600 °C for 3 min, T_2=1450 °C for 6 h) and (c) CS_3 regime (1450 °C for 6 h).

Pre-sintering at T_1 was important because of the critical density obtained during the first step sintering. Without pre-sintering at T_1, the density of the sample was below the critical density, particle coarsening and repacking were the mechanisms responsible for densification [5]. Although the grain growth was achieved by GBD, which typically had lower activation energy than GBM, some repacking events could require more robust kinetics available only at a higher temperature. If the sample was firstly sintered at a higher T_1 and a critical density was reached, the pores become subcritical and unstable and can be filled as long as GBD was allowed. Therefore, a lower T_2 would suffice as long as it was not too low to exhaust diffusion [36]. It could also be seen from Fig. 6 that fracture surfaces of the samples under different sintering regimes were characterized by a mixed mode of intergranular and transgranular fracture but dominated by the transgranular fracture mode.

3.5. Phase transformation in two step sintering process

Phase transformation of Al_2O_3 starting material composed of amorphous Al_2O_3, boehmite (AlOOH) and χ-Al_2O_3 during TSS process was investigated. As shown in Fig. 7, peaks of α-Al_2O_3 were observed in the samples hot pressed at 1600 °C for 3 min, indicating that transitional Al_2O_3 and amorphous Al_2O_3 were transformed to α-Al_2O_3 during the first step sintering. This agreed with the results of our previous work as reported in [25], for the samples hot pressed under CS regime, with the increased sintering temperature, amorphous Al_2O_3 and AlOOH transformed to γ when the as milled powders were sintered at 961 °C for 90 min, and all the transitional Al_2O_3 and amorphous Al_2O_3 were transformed to α-Al_2O_3 completely when the premixed powders were sintered at 1100 °C for 90 min.

The differences was that the sintering temperature used to investigate the phase transformation during TSS was higher but the holding time was shorter than that reported in [25], revealing that although both the sintering temperature and holding time were important factors of the sintering process, the influence of sintering temperature on the phase transformation of Al_2O_3 was much more obvious than that of holding time, and the transformation process during the TSS process probably occurred through the same path as in the CS process. According to [25], phase transformation of the transitional Al_2O_3 could result in smaller grain size of α-Al_2O_3. For the samples under TSS regimes, smaller initial gain size was beneficial to the obtaining of small final grain size. As second phase toughening particles, smaller particle size of Al_2O_3 could lead to better toughening effect for WC–40 vol% Al_2O_3 composites. As a result, phase transformation of Al_2O_3 during TSS was a positive factor to the improvement of mechanical properties of WC–40 vol% Al_2O_3 composites.

3.6. Mechanical properties

Mechanical properties of WC–40 vol% Al_2O_3 composites sintered under CS and TSS regimes were shown in Table 2. It could be seen that the Vickers hardness, fracture toughness and flexural strength of the samples consolidated under the TSS_4 regime were higher than that of the samples sintered under the CS_1 and other TSS regimes. The improvement of mechanical properties could be due to the contribution of smaller grain size and improved relative densities to them.

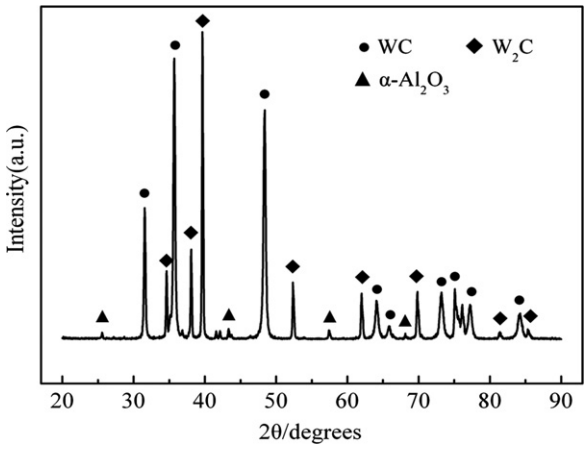

Fig. 7. XRD patterns of WC–40 vol% Al_2O_3 composites sintered at 1600 °C for 3 min.

A well known empirical dependence of hardness on porosity and grain size for ceramics is given by [37]

$$\mathrm{HV} = Kd^{-a}e^{-bp} \tag{2}$$

where HV is the Vickers hardness; d is grain size; p is porosity in the specimen, its variation is from 1% to 4%; K, a and b are empirical constants, a can be approximated to be 0.5 [37]. From the non-linear curve fitting results using Matlab, the variation of K is from 29.23 to 51.42, the variation of b is from −0.55 to 17.04. It can be indicated that the grain size and porosity of the samples were the most effective criteria for the final values of the hardness. It could be illustrated that the hardness of samples consolidated under TSS_2 regime did not be improved obviously compared with that of the samples sintered under the CS_1 regime attributed to its lower relative density and larger grain size, as illustrated in Fig. 3c and Fig. 4.

For the samples under TSS_3, the relative densities were improved, however, the grain growth was observed. At the initial sintering stage at T_2, the increase in relative density was a dominating factor for the increase of Vickers hardness; while in the final sintering stage, the deteriorate effect of grain growth overweighed the positive influence of the improved relative density, as a result, the Vickers hardness decreased. As to the samples under TSS_4, the highest Vickers hardness did strongly depend on the nearly full density and inhibited grain growth.

Fracture toughness is a property that materials resist to the propagating cracks. Accordingly, the higher volume of grain boundaries could effectively hinder the crack propagation, and dense and refined microstructure were benefit for the improvement of it. Fig. 8 indicated the FE-SEM images of Vickers indentation crack extension path of WC–40 vol% Al_2O_3 composites consolidated under TSS_4 regime. It can be seen that the crack width was narrow and many crack deflections and crack bridges were observed. These effects required more external load to force the crack to propagate further improving the fracture toughness and the flexural strength. As a result, the fracture toughness varied from 10.43 to 12.00 MPa $m^{1/2}$.

The flexural strength represented the similar trend like the influence of grain size and relative density variation on the Vickers hardness, because flexural strength also had close relationship with porosity and grain size of the samples as follows [38]

$$\sigma = \sigma_0 \exp(-k_1\alpha) \tag{3}$$

$$\sigma = \sigma_0 + k_2 d^{-m} \tag{4}$$

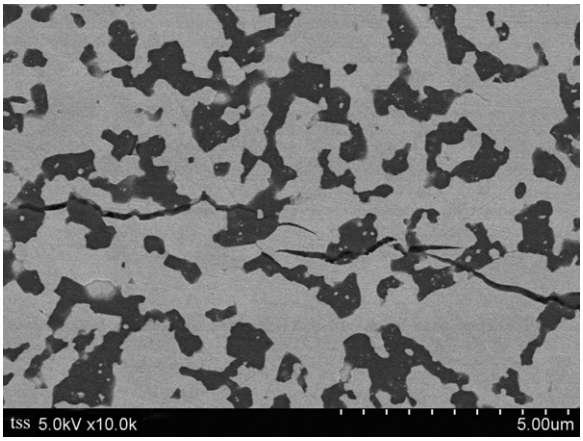

Fig. 8. FE-SEM image of Vickers indentation crack extension path of WC–40 vol% Al_2O_3 composites consolidated under TSS_4 regime.

where σ is the flexural strength; d is grain size; α is residual porosity, its variation is from 1% to 4%; σ_0 is the flexural strength of materials without defect, its best non-linear curve fitting result is 1347 MPa; k_1, k_2 and m are experimental coefficients, the variation of k_1 is from 4.83 to 7.34, the variation of k_2 is from -696.1 to 34.07, the variation of m is from -1.29 to 0.72. This equation indicated that the flexural strength would increase with the decreasing porosity, this agreed with the lower flexural strength of samples under TSS_2 regime. For the samples under the TSS regime (TSS_3 and TSS_4), with the increasing holding time at T_2, the decrease of porosity was obviously benefit to the flexural strength; however, at the final stage of sintering, the relative density of the samples was almost constant, the flexural strength of the samples would be controlled by grain size. If the sintering regime was not

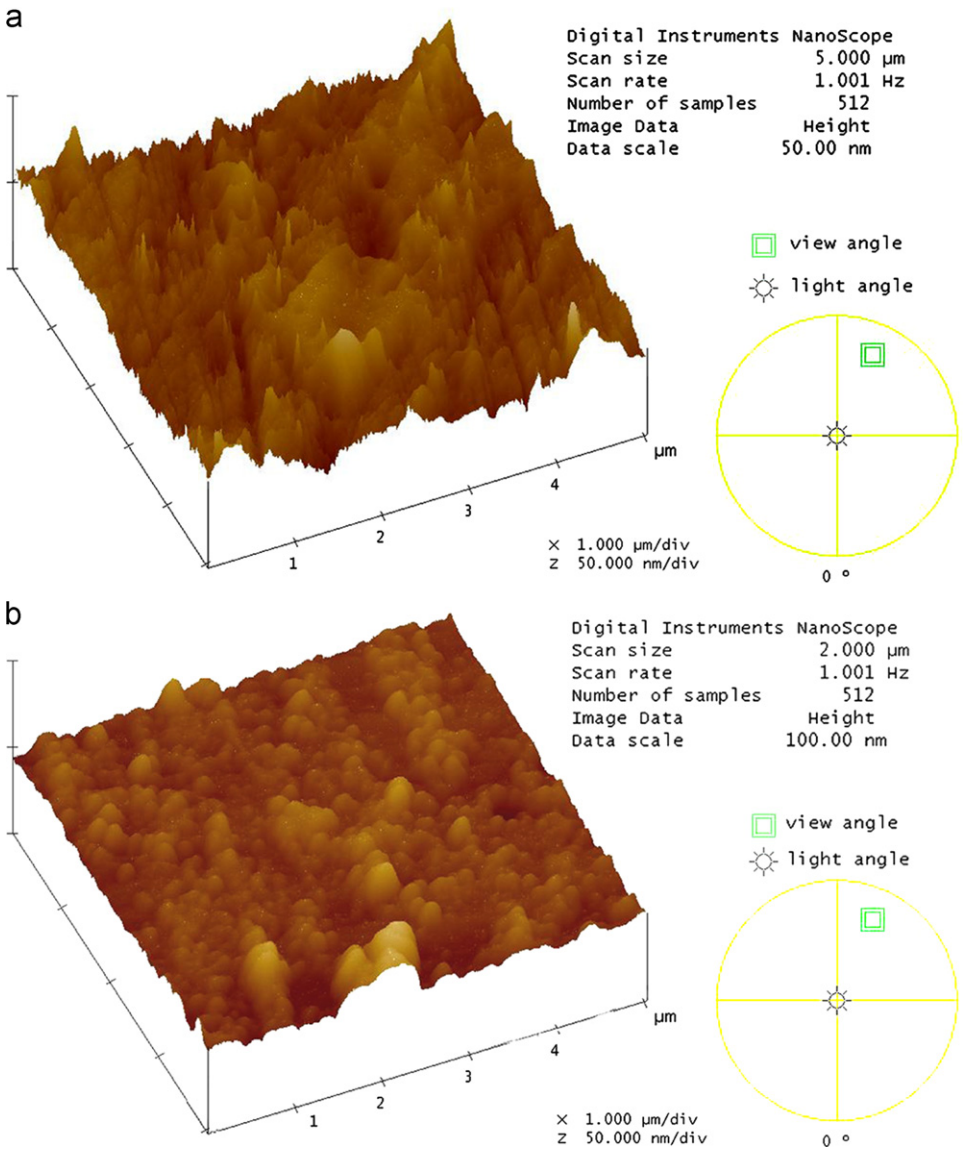

Fig. 9. 3D SPM images showing the particulate/matrix interfacial microstructures of (a) CS_1 regime (1540 °C for 90 min) and (b) TSS_4 regime (T_1 = 1600 °C for 3 min, T_2 = 1450 °C for 6 h).

proper, for example the TSS_3 regime with higher T_2, longer holding time led to the quick and irregular grain growth, which was one of the reasons causing the reduction of flexural strength. While in the TSS_4 regime, grain growth could be effectively inhibited during the final stage of sintering, resulting in the enhanced flexural strength.

The 3D SPM images were made on the polished surface of the composites to clarify further toughening effect responsible for the enhanced flexural strength. Fig. 9 shows the particulates/matrix interfacial microstructure of the samples sintered under CS_1 and TSS_4 regimes. It can be seen that, the morphology of the samples obtained under CS_1 regime was rough and fluctuated, as shown in Fig. 9a, which was due to the large and incompletely separated Al_2O_3 toughening particulates. However, under the TSS_4 regime, the SPM image presented in a much more smoothened and dispersed appearance, and the Al_2O_3 toughening particulates had continuous and compatible interfaces with the matrix, as can be seen in Fig. 9b. In addition to the refined and nearly full dense microstructure, the flexural strength was greatly enhanced from 756 to 1285 MPa. The flexural strength was comparable with that of the WC–(3–8) wt% Co cemented hard alloys (1150–1650 MPa) [39].

4. Conclusions

(1) The feasibility of two step sintering method to the WC–40 vol% Al_2O_3 composites was demonstrated and the optimum TSS regime was investigated. The first step temperature (T_1) was selected comprehensively according to the densification rate and grain size during the conventional sintering. The second step temperature (T_2) was chose according to the relative density, grain size and mechanical properties of the TSS regimes.

(2) Two step sintering conducted at $T_1=1600\ ^\circ C$ and $T_2=1450\ ^\circ C$ (TSS_4) significantly prohibited the grain growth in the final stage of hot pressing of WC–40 vol% Al_2O_3 composites without deteriorating the densification process. Under TSS regimes with a lower second step temperature (1400 °C), a relative density of only 96%TD was observed even the holding time increased to 6 h due to the surface diffusion, while under TSS regimes with a higher second step temperature (1500 °C), a noticeable grain size of 5.00 μm was obtained.

(3) When the as milled WC–40 vol% Al_2O_3 powders were hot pressed under TSS_4 regime, a relative density of 99% and a grain size of 2.38 μm were obtained, and an excellent Vickers hardness of 19.71 GPa was achieved, combining a fracture toughness of 12 MPa $m^{1/2}$ with an acceptable flexural strength of 1285 MPa. Compared with the nearly full densified samples consolidated under CS_1 regime (1540 °C for 90 min), the grain size decreased (2.79 μm for the CS_1 sample), the Vickers hardness, fracture toughness and the flexural strength were all improved (18.65 GPa, 10.43 MPa $m^{1/2}$, 756 MPa for the CS_1 sample) due to the refined microstructure and the transgranular fracture mode.

Acknowledgments

The authors would like to acknowledge the financial support provided by Shanghai Leading Academic Discipline Project under project no. B602, and the support by the Nanomaterials Research Special Foundation of Shanghai Science and Technology Committee under grant no. 05nm05031.

References

[1] M.L. Huckabee, H. Palmour III, Rate controlled sintering of fine-grained Al_2O_3, American Ceramic Society Bulletin 51 (1972) 574–576.
[2] H. Palmour III, M.L. Huckabee, T.M. Hare, Microstructural development during optimized rate controlled sintering, in: R.N. Fulrath, J.A. Parks (Eds.), Ceramic Microstructure, Westview Press, Boulder CO, 1977, pp. 308–319.
[3] H. Palmour, Rate-controlled sintering for ceramics and selected powder metals, in: D.P. Uskovic, H. Palmour, R.M. Spiggs (Eds.), Science of Sintering, Plenum Press, New York, 1989, pp. 337–356.
[4] I.W. Chen, X.H. Wang, Sintering dense nanocrystalline ceramics without final-stage grain growth, Nature 404 (2000) 168–171.
[5] X.H. Wang, P.L. Chen, I.W. Chen, Two-step sintering of ceramics with constant grain-size. I. Y_2O_3, Journal of the American Ceramic Society 89 (2006) 431–437.
[6] X.H. Wang, X.Y. Deng, H.L. Bai, H. Zhou, W.G. Qu, L.T. Li, I.W. Chen, Two-step sintering of ceramics with constant grain-size. II. $BaTiO_3$ and Ni–Cu–Zn ferrite, Journal of the American Ceramic Society 89 (2006) 438–443.
[7] M. Mazaheri, A.M. Zahedi, S.K. Sadrnezhaad, Two-step sintering of nanocrystalline ZnO compacts: effect of temperature on densification and grain growth, Journal of the American Ceramic Society 91 (1) (2008) 56–63.
[8] M. Mazaheri, Z. Razavi Hesabi, S.K. Sadrnezhaad, Two-step sintering of titania nanoceramics assisted by anatase-to-rutile phase transformation, Scripta Materialia 59 (2008) 139–142.
[9] M. Mazaheri, M. Valefi, Z. Razavi Hesabi, S.K. Sadrnezhaad, Two-step sintering of nanocrystalline $8Y_2O_3$ stabilized ZrO_2 synthesized by glycine nitrate process, Ceramics International 35 (2009) 13–20.
[10] M. Mazaheri, A. Simchi, F. Golesatani-Fard, Densification and grain growth of nanocrystalline 3Y-TZP during two-step sintering, Journal of the European Ceramic Society 28 (2008) 2933–2939.
[11] Z.R. Hesabi, M. Haghighatzadeh, M. Mazaheri, D. Galusek, S.K. Sadrnezhaad, Suppression of grain growth in sub-micrometer alumina via two step sintering method, Journal of the European Ceramic Society 29 (2009) 1371–1377.
[12] G.F. Farhad, M. Mazaheri, M. Aminzare, T. Ebadzadeh, Microstructural evolution of a commercial ultrafine alumina powder densified by different methods, Journal of the European Ceramic Society 31 (14) (2011) 2593–2599.
[13] C.J. Wang, C.Y. Huang, Y.C. Wu, Two step sintering of fine alumina-zirconia ceramics, Ceramics International 35 (2009) 1467–1472.
[14] Z.H. Chen, J.T. Li, J.J. Xu, Z.G. Hu, Fabrication of YAG transparent ceramics by two-step sintering, Ceramics International 34 (2008) 1709–1712.
[15] Z. Li, Z. Li, A. Zhang, Y.J. Zhu, Synthesis and two-step sintering behavior of sol–gel derived nanocrystalline corundum abrasives, Journal of the European Ceramic Society 29 (2009) 1337–1345.

[16] K. Maca, V. Pouchly, P. Zalud, Two-step sintering of oxide ceramics with various crystal structures, Journal of the European Ceramic Society 30 (2010) 583–589.
[17] M.H. Fathi, M. Kharaziha., Two-step sintering of dense, nanostructural forsterite, Materials Letters 63 (2009) 1455–1458.
[18] Z.G. Zhang, Y.H. Liu, G.C. Yao, G.Y. Zu, D. Wu, Y. Hao, Synthesis and characterization of dense and fine nickel ferrite ceramics through two-step sintering, Ceramics International 38 (2012) 3343–3350.
[19] M. Lukica, Z. Stojanovia, S.D. Skapinb, M. Macek-Krzmancb, M. Mitricc, S. Markovica, D. Uskokovic., Dense fine-grained biphasic calcium phosphate (BCP) bioceramics designed by two-step sintering, Journal of the European Ceramic Society 31 (2011) 19–27.
[20] M. Mazaheri, A.M. Zahedi, M. Haghighatzadeh, S.K. Sadrnezhaad, Sintering of titania nanoceramic: densification and grain growth, Ceramics International 35 (2009) 685–691.
[21] S.H. Kim, J.W. Kim, T.S. Jo, Y.D. Kim, High coercive Nd–Fe–B magnets fabricated via two-stepsintering, Journal of Magnetism and Magnetic Materials 323 (2011) 2851–2854.
[22] J. Ma, S.G. Zhu, C.X. Ouyang, Two step hot pressing sintering of nanocomposite WC–MgO compacts, Journal of the European Ceramic Society 31 (2011) 1927–1935.
[23] Y.I. Lee, Y.W. Kim, M. Mitomo, D.Y. Kim, Fabrication of dense nanostructured silicon carbide ceramics through two-step sintering, Journal of the American Ceramic Society 86 (2003) 1803–1805.
[24] D.Y. Yang, D.Y. Yoon, Suk-Joong, L. Kang, Suppression of abnormal grain growth in WC–Co via two step liquid phase sintering, Journal of the American Ceramic Society 94 (4) (2011) 1019–1024.
[25] H.X. Qu, S.G. Zhu, Q. Li, C.X. Ouyang, Influence of sintering temperature and holding time on the densification, phase transformation, microstructure and properties of hot pressing WC–40 vol% Al_2O_3 composites, Ceramics International 38 (2012) 1371–1380.
[26] H.X. Qu, S.G. Zhu, P. Di, C.X. Ouyang, Q. Li, Microstructure and mechanical properties of WC–40 vol% Al_2O_3 composites hot pressed with MgO and CeO_2 additives, Ceramics International 39 (2013) 1931–1942.
[27] S.C. Carniglia, Reexamination of experimental strength vs grain size data for ceramics, Journal of the American Ceramic Society 55 (1972) 243–247.
[28] A.A. Griffith, The phenomena of rupture and flow in solids, Philosophical Transactions of the Royal Society of London 221A (1920–1921) 163–198.
[29] D.K. Shetty, I.G. Wright, P.N. Mincer, A.H. Clauer, Indentation fracture of WC–Co cermets, Journal of Materials Science 20 (1985) 1873–1882.
[30] P. Duran, F. Capel, J. Tartaj, C. Moure, Sintering behavior and electrical properties of nanosized doped-ZnO powders produced by metallorganic polymeric processing, Journal of the American Ceramic Society 84 (2001) 1661–1668.
[31] R.J. Brook, Controlled grain growth, in: F.F.Y. Wang (Ed.), Treatise on Materials Science and Technology, vol. 9, Academic Press New York, 1976, pp. 331–395.
[32] P.L. Chen, I.W. Chen, Sintering of fine oxide powder: II: sintering mechanisms, Journal of the American Ceramic Society 80 (3) (1997) 637–645.
[33] J.H. Zhao, M.P. Harmer, Effect of pore distribution on microstructure development: I, matrix pores, Journal of the American Ceramic Society 71 (2) (1988) 113–120.
[34] J.H. Zhao, M.P. Harmer, Effect of pore distribution on microstructure development: II, first- and second-generation pores, Journal of the American Ceramic Society 71 (7) (1988) 530–539.
[35] J.H. Zhao, M.P. Harmer, Effect of pore distribution on microstructure development: III, model experiments, Journal of the American Ceramic Society 75 (4) (1992) 830–843.
[36] K. Bodisova, P. Sajgalik, D. Galusek, P. Svancarek, Two step sintering of alumina with submicrometer grain size, Journal of the American Ceramic Society 90 (1) (2007) 330–332.
[37] A.A. Mahday, M.S. El-Eskandarany, H.A. Ahmed, A.A. Amer, Mechanically induced solid state carburization for fabrication of nanocrystalline ZrC refractory material powders, Journal of Alloys and Compounds 299 (2000) 244–253.
[38] W.D. Kingery, Introduction to Ceramics, Wiley, New York, 1976, p. 411.
[39] Z.H. Qiao, X.F. Ma, W. Zhao, H.G. Tang, B. Zhao, Nanostructured novel cemented hard alloy obtained by mechanical alloying and hot pressing sintering and its applications, Journal of Alloys and Compounds 462 (2008) 416–420.